Microstructure and Mechanical Property of Al-Cu-Li Alloy Joint by Laser Welding with Filler Wire

LI Kang, WANG Shaogang, HU Bingzhou*

College of Materials Science and Technology, Nanjing University of Aeronautics and Astronautics, Nanjing 211106, P. R. China

(Received 8 September 2021; revised 6 January 2022; accepted 23 February 2022)

Abstract: The Al-Cu-Li alloy is welded by using laser beam welding, and the welding wire ER4043 is used as filler metal. The microstructure and mechanical property of welded joints are systematically investigated. Microstructure analyses show that the fusion zone is mainly composed of α-Al matrix phase and some strengthening phases including T, δ′, θ′, β′ and T_1, etc. During welding, the weld formation and joint quality are obviously improved by the addition of Al-Si filler wire. The measurements of mechanical property indicate that, compared with that of the base metal (BM), the microhardness in the weld zone is decreased to a certain extent. Under the appropriate welding parameters, the tensile strength of welded joint reaches 369.4 MPa, which is 67.8% of that of the BM. There are many dimples on the joint fracture surface, and it mainly presents the fracture characteristic of dimple aggregation.

Key words: Al-Cu-Li alloy; laser welding with filler wire; microstructure; mechanical property

CLC number: TG456.7 **Document code:** A **Article ID:** 1005-1120(2022)03-0358-09

0 Introduction

Al-Li alloy has excellent comprehensive property such as low density, high specific strength and specific stiffness, and good formability, and they are widely used in aerospace field[1]. Because they are often used as welded structure, some welding procedures such as friction stir welding (FSW) were used to weld these alloys[2]. Compared with that of the fusion welding, the process flexibility of FSW is insufficient, and it is difficult to weld the component with complex shape. During the aircraft manufacturing process, if the riveted structure was replaced by the laser-welded structure, the structural weight and production cost could be greatly reduced[3]. At present, the laser beam welding (LBW) of Al-Li alloy has been paid more attention. As an advanced welding technology, the LBW was also used to weld the high-silicon aluminum alloy and the aluminum matrix composite, respectively[4-5]. Moreover, the LBW of newly developed materials and dissimilar materials were increasingly applied, for example, the LBW of high temperature shape memory alloys such as precipitation strengthened Ni-rich NiTiHf and H-phase strengthened Ni-rich NiTi-20Zr, and the dissimilar LBW of a CoCrFeMnNi high entropy alloy to 316 stainless steel[6-8].

Examilioti et al.[9] studied the effect of laser welding parameters on the weld formation of 2198 Al-Li alloy. With the increase of laser power, the morphology of weld cross section changed from narrow V shape to Ⅰ shape. The 2060 Al-Li alloy was welded by using LBW, and the effect of welding parameters on weld formation, porosity and microhardness was investigated[10]. Cui et al.[11] analyzed the microstructure of LBW joint of Al-Li alloy. Liu et al.[12] conducted the LBW of 2060 alloy, and the relationship between microstructure and mechanical property of the joint was investigated.

Because the active element Li was added to the Al-Li alloy, it was prone to generating welding defects such as weld porosity and hot cracking during

*Corresponding author, E-mail address: sgwang@nuaa.edu.cn.

How to cite this article: LI Kang, WANG Shaogang, HU Bingzhou. Microstructure and mechanical property of Al-Cu-Li alloy joint by laser welding with filler wire[J]. Transactions of Nanjing University of Aeronautics and Astronautics, 2022, 39(3): 358-366.

http://dx.doi.org/10.16356/j.1005-1120.2022.03.010

welding[13]. The 2198 alloy was welded by using LBW[14], and the susceptibility to hot cracking could be decreased to a certain extent by preheating, preloading and optimizing welding parameters. Here, preloading means that a compressive load was added to the weldment during welding, the effect of strain localization due to solidification shrinkage would be reduced or even compensated. Compared with that of the autogenous LBW, some alloying elements can be added to the weldment during laser welding with filler wire. The chemical composition of weld metal can be adjusted, and the morphology and distribution of low melting point eutectic are improved, thus the hot cracking in Al-Li alloy weldment is greatly decreased. In the 2195 Al-Li alloy laser-welded joint, the susceptibility to hot cracking was obviously decreased by using the Al-Si filler metal, which could increase the amount of eutectic structure and improve the fluidity of molten pool[15]. Lukin et al.[16] stated that the hot cracking in the 1420 Al-Li alloy joint could be effectively reduced by the addition of Al-Mg filler wire. The AlSi12 filler wire was used to weld the 2060 alloy, and the irregular distribution of LiAlSi phase in weldment could contribute to breaking the Al_2Cu eutectic phase at grain boundary, thus the joint mechanical property was improved[17]. The Al-Li alloy joint by the addition of new CW3 filler wire had higher tensile strength and lower susceptibility to hot cracking[18].

At present, investigation on the laser welding with filler wire for the Al-Cu-Li alloy is still not systematic and in-depth. It is necessary to investigate the welding technological characteristics and the effect of filler wire on the microstructure and property of the welded joint. In present work, the Al-Si filler wire is used to weld the Al-Cu-Li alloy. The effect of welding parameters on the microstructure and mechanical property of the welded joint is investigated, and some results can be provided for the application of the welded structure.

1 Materials and Procedure

The base metal (BM) is the Al-Cu-Li alloy plate and its heat treatment condition is T8 (solution treatment, cold working and then artificial aging). The BM is machined to welding sample with the dimensions of 150 mm × 50 mm × 4 mm. The joint type is butt joint. The filler metal is ER4043 welding wire with the diameter of 1.2 mm. The chemical composition of BM and filler wire is listed in Table 1.

Table 1 Chemical composition of base metal and filler wire (in weight) %

Alloy	Cu	Mg	Li	Zr	Ag	Ti	Si	Al
BM	4.05	0.38	0.96	0.13	0.31	0.06		Bal.
ER4043	<0.01	<0.01				<0.01	5.2	Bal.

Before welding, the welding samples are pretreated to remove thoroughly the oxide film and grease contamination on the sample surface. The laser beam welding machine is TruDisk-12003 type disc laser with the maximum output power of 12 kW. The KUKA KR30HA type welding robot is used to control the angle and movement of the incident laser beam during welding. The equipment of laser welding with filler wire is shown in Fig.1. Welding is carried out along the longitudinal direction of the sample, and the angle between the laser beam and vertical direction is 10°. After some attempt welding, combined with the observation of weld formation and the measurement of joint performance, the welding procedure is determined. The amount of defocus is 0 mm and the wire feeding speed is 5 m/min. In order to avoid oxidation and reduce the weld porosity, argon gas is used to protect the top and the root of the joint during welding. The argon purity is 99.99%, and the gas flow rate is 15 L/min and 10 L/min. The main parameters of laser welding with filler wire for the Al-Cu-Li alloy are given in Table 2.

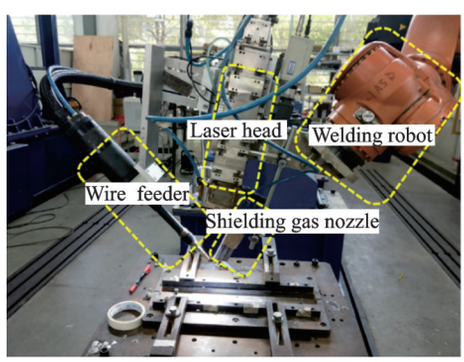

Fig.1 Equipment of laser welding with filler wire

Table 2 Parameters of laser welding with filler wire for the Al-Cu-Li alloy

Sample No.	Laser power / kW	Welding speed / ($m \cdot min^{-1}$)	Heat input / ($J \cdot mm^{-1}$)
1#	4.5	3.0	90
2#	4.5	3.5	77
3#	4.5	4.5	60
4#	4.0	3.5	69
5#	5.0	3.5	86

After welding, the microstructure of the welded joint is observed by using Leica DMILM inverted optical microscope. The chemical composition of micro-region in weldment is analyzed by using energy dispersive spectrometer (EDS). The phase constituent of the weld metal is identified by using D8 Advance type X-ray diffractometer (XRD). The precipitated phases in weldment are observed by using JEM-2100F type transmission electron microscope (TEM). The TEM specimen is prepared by the following steps: Mechanically grinding to the thickness of about 50 μm, and then punching thin foils with the diameter of 3 mm, and double-jet electrolytic thinning with the electrolyte of 30% nitric acid methanol solution (volume ratio). The microhardness in the weld zone is measured by using HXS-1000AC type hardness tester with the load of 200 g and the duration time of 15 s. The tensile property of the welded joint is tested by using CMT-5105 type electronic universal material testing machine with the loading rate of 1 mm/min. The fracture morphology of the joint is observed by using JSM-6360LV type scanning electron microscope (SEM), and the tensile fracture characteristic of the joint is analyzed.

2 Results and Discussion

2.1 Weld morphology and microstructure

The macrographs of welded joints under different welding parameters are shown in Fig. 2. Due to the relatively low laser power, the incomplete penetration is generated to joint 4#. Compared with those of the other joints, the weld formation of joint 2# is good, and no welding defects such as undercut and lack of fusion are generated in the weldment. Consequently, the appropriate welding parameters are determined. Fig. 3 shows the cross section morphology and microstructure of joint 2#. During the welding of the Al-Cu-Li alloy, hot cracking was probably occurred in weldment[13]. Moreover, in the autogenous LBW process, due to the feature of the Al-Li alloy and the evaporation and burning loss of alloying elements, the welding defects such as underfill and undercut were easily generated[9]. In present work, the Al-Si filler wire is added during LBW, and the weld formation is obviously improved. As shown in Fig.3(a), the joint with good morphology is ob-

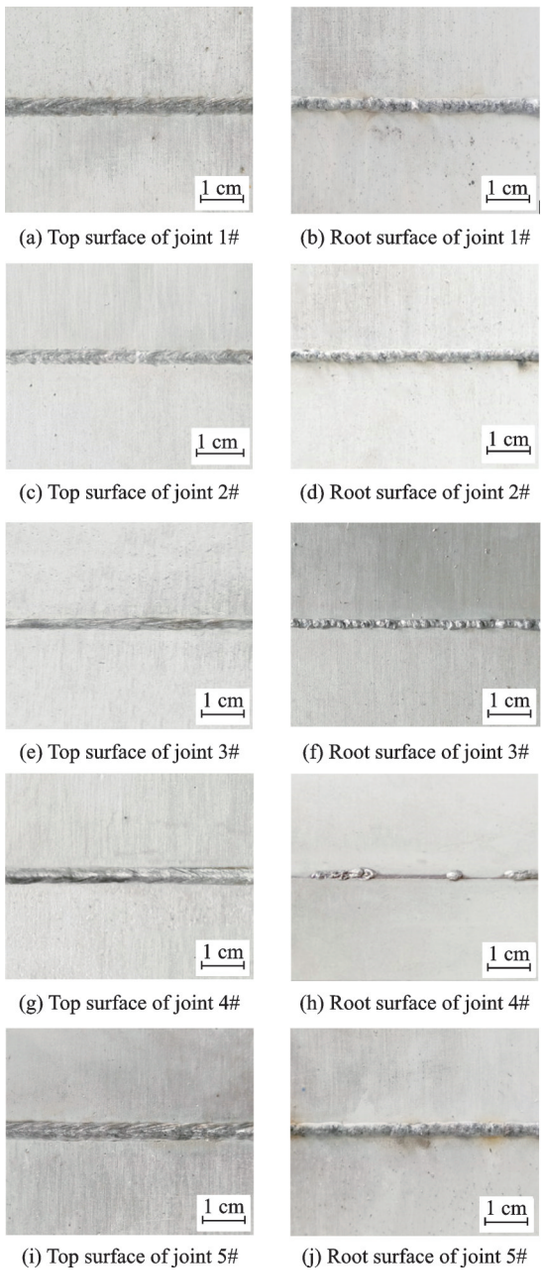

Fig.2 Macrographs of welded joints

tained, no welding defects such as gas pores and micro-cracks are produced, which is advantageous to the mechanical property of the welded joint.

The microstructure of BM is shown in Fig.3 (b). It is the strip rolled structure with preferential orientation, and many strengthening phases distribute within grain and at grain boundary. The main strengthening phases in Al-Cu-Li alloys were T_1 (Al_2CuLi), δ' (Al_3Li) and θ' (Al_2Cu) phases[19]. There is a fine equiaxed grain zone (EQZ) between the fusion zone (FZ) and heat-affected zone (HAZ), and the grain size in EQZ is 4—8 μm, as shown in Fig.3(c). The formation mechanism of EQZ had studied by many researchers. Reddy et al.[20] stated that the grain morphology in BM basically had no effect on the formation of EQZ. The Al_3Zr(β') particles only existed in EQZ, and the β' particles played an important role on the formation of EQZ. Gutierrez and Lippold[21] concluded that the formation of EQZ was mainly due to the heterogeneous nucleation of Al_3Zr and Al_3(Li, Zr) particles. From fusion line (FL) to weld center, the grain morphology in FZ changs from columnar crystal to equiaxed dendrite. During welding, the columnar crystals nucleate at the surface of EQZ grains and grow towards the FZ by the pattern of epitaxial growth. With the growth of columnar crystals, the temperature gradient in FZ is gradually decreased. The large constitutional supercooling is generated, thus the equiaxed dendrites are formed in the weld center, as shown in Fig.3(d).

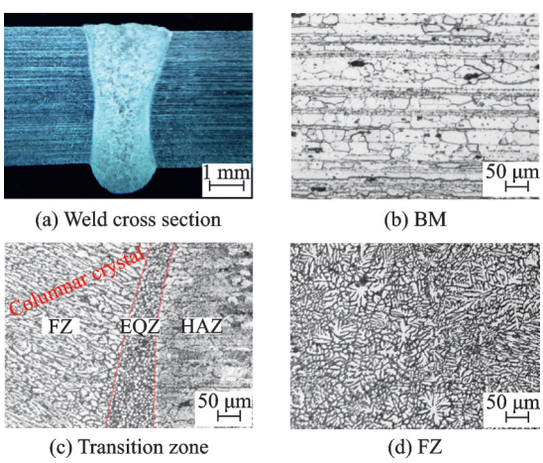

(a) Weld cross section (b) BM (c) Transition zone (d) FZ

Fig.3 Morphology and microstructure of joint 2#

Fig.4 shows the microstructure of the joint transition zone (TZ) under different welding parameters. The grain size in EQZ is basically the same. With the decrease of heat input, the width of EQZ decreases. The average width of EQZ in the middle part of joint 1#, joint 2# and joint 3# is 88 μm, 72 μm and 34 μm, respectively, as shown in Figs.4 (b, e, h). It was consistent with the results in Ref.[21]. Under the condition of different heat inputs, for the joint 1#, joint 2# and joint 3#, the average width of HAZ is 3.3 mm, 2.5 mm and 1.7 mm, respectively, and the average width of FZ is 2.0 mm, 1.8 mm and 1.5 mm, respectively.

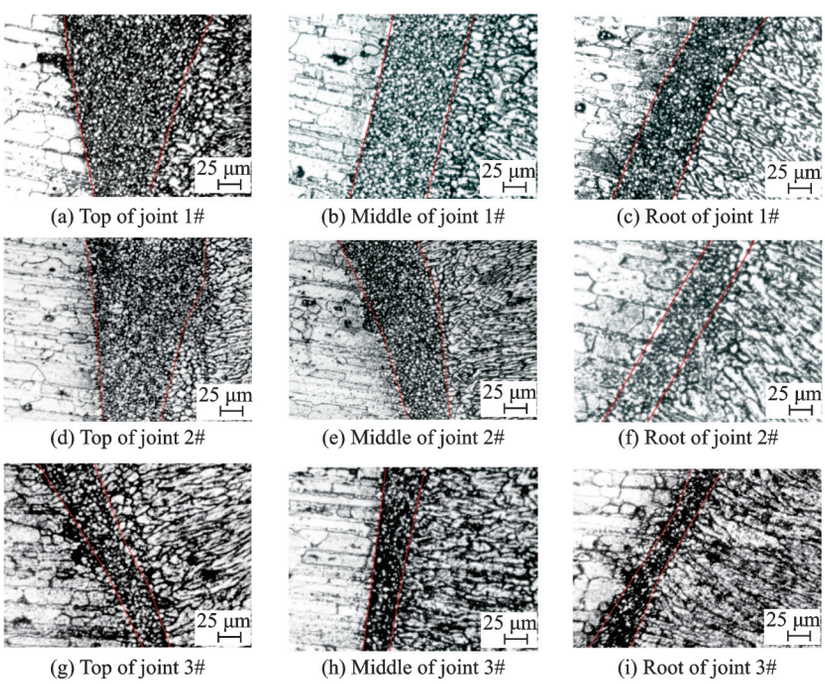

(a) Top of joint 1# (b) Middle of joint 1# (c) Root of joint 1#
(d) Top of joint 2# (e) Middle of joint 2# (f) Root of joint 2#
(g) Top of joint 3# (h) Middle of joint 3# (i) Root of joint 3#

Fig.4 Microstructures of the joint transition zone

Liu et al.[12] found that the width of EQZ in the middle part of the 2060 alloy joint by LBW was the maximum, while those in the upper and lower parts were relatively narrow, which was related to the combination effect of thermal buoyancy and Marangoni convection. As a result, the width of EQZ in different regions was different from that of the joint by autogenous LBW. The microstructures of joint 1# at the top, middle and root are shown in Figs. 4(a—c), respectively. The width of EQZ in the upper part of joint 1# is the maximum, and its average width is 110 μm and the maximum width 169 μm. The average width of EQZ is 88 μm in the middle part. The EQZ is the narrowest in the lower part, and its average width is 72 μm.

2.2 Distribution of alloying elements and phase constituent

Fig.5(a) shows the SEM image of FZ, and it is mainly composed of eutectic structure. Some secondary phases precipitate at the grain boundaries, and there is few strengthening phase within the grain. As shown in Fig.5(a), EDS analysis is carried out along the line scanning path (red line). The distribution curves of alloying elements Al, Cu, Si and Mg are shown in Fig.5(b). The contents of elements Si and Cu increase greatly at grain boundaries, while their contents within grains decrease obviously. The content of element Cu or Si increases correspondingly in the region with the lower content of element Al. The distribution of element Mg uniforms relatively. During the fusion welding of the aluminum alloy, the low melting point eutectic is prone to aggregation at grain boundary to form liquid film. Hot cracking was easily to generate in weldment under the action of the welding stress[13]. In present work, by the addition of Al-Si filler wire, the amount of eutectic structure increases. Moreover, the fluidity of the molten pool is greatly improved. Due to the effect of crack healing, the hot cracking is effectively avoided in weldment.

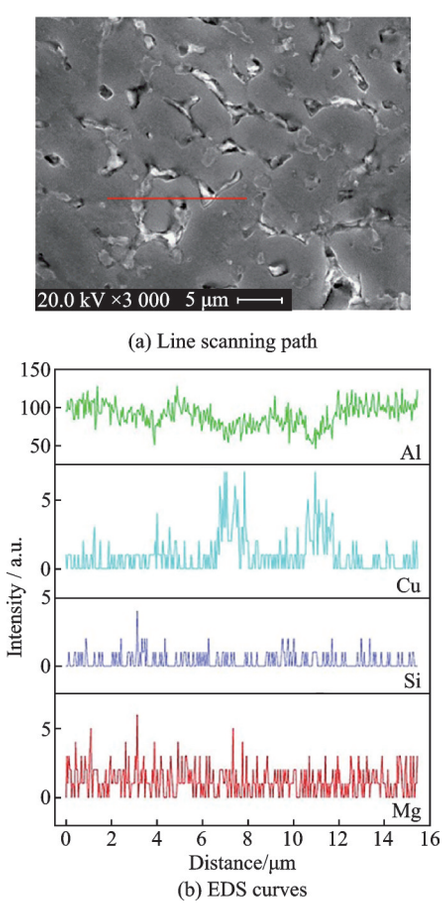

Fig.5 SEM image of FZ and EDS analysis

XRD analysis of the weldment is carried out, and the result is shown in Fig.6. There are mainly α-Al matrix phase and some strengthening phases such as T_1 (Al_2CuTi), T (AlLiSi), δ′ (Al_3Li), θ′ (Al_2Cu) and β′ (Al_3Zr) in the weldment. In the welding process, the rapid cooling of the molten pool easily leads to segregation of alloying elements in weldment. During the welding of Al-Cu-Li alloys, alloying elements, especially Cu element, were prone to segregation at the dendrite and grain boundaries[22], thus the supersaturation degree of alloying elements in weldment was probably insufficient. In the subsequent natural aging process, the quantity of precipitated phases in weldment is not enough, which leads to the softening effect in the

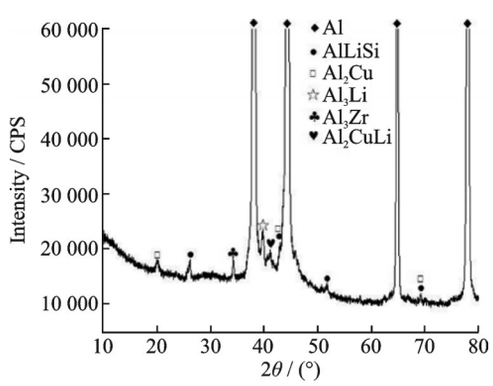

Fig.6 XRD analysis pattern of the weldment

weld zone.

TEM images of the precipitated phases in weldment are shown in Fig.7. Combined with the chemical composition of BM and the result of XRD analysis, the different precipitated phases can be inferred. As shown in Fig.7(a), the triangular strengthening phase is the T (AlLiSi) phase[17-18]. The formation temperature of T phase is higher, the Si-rich phase is easily to aggregate and grow. The acicular strengthening phase is the T_1(Al_2CuTi) phase[23-24], as shown in Fig.7(b). The T_1 phase is the main strengthening phase in the Al-Cu-Li alloy. Due to the semi-coherent relationship between the T_1 phase and α-Al matrix, there is a large mismatch between them. The movement of dislocations will be inhibited to a certain extent, thus good strengthening effect is generated. The bulk strengthening phase is the β′(Al_3Zr) phase[25], as shown in Fig.7(c). The existence of β′ phase contributes to form the EQZ in the welded joint.

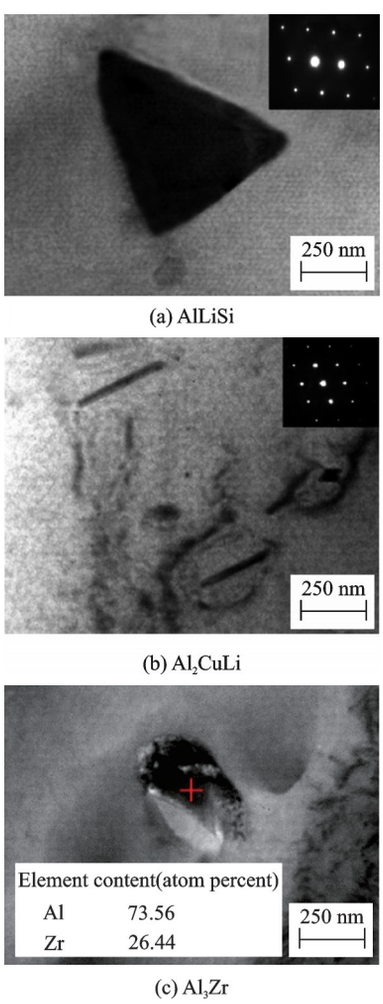

Fig.7 TEM images of precipitated phases in weldment

2.3 Microhardness distribution

The microhardness distribution curve of joint 2# is shown in Fig.8. The hardness distribution in the weld zone presents the shape of "V". The average hardness in FZ is 115 HV, and it is lower than those of HAZ (145 HV) and BM (170 HV). Softening effect occurs to the Al-Cu-Li alloy joint, and FZ is the weak area of the joint. In as-welded (AW) condition, the weld metal is under-aging, and the quantity of precipitated phases is less, thus the hardness in FZ decreases obviously.

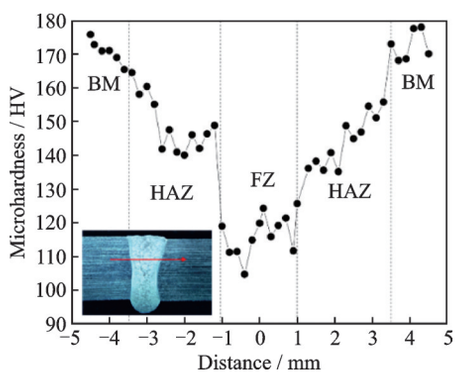

Fig.8 Microhardness distribution of joint 2#

Due to the effect of the weld thermal cycle, the strengthening phases in HAZ aggregate and grow, the quantity of strengthening phases decreases, and the spacing among them increases. According to the Orowan mechanism, the strengthening effect of secondary phases is inversely proportional to the spacing among strengthening particles. The effect of precipitation strengthening weakens, as a result, the hardness in HAZ decreases to a certain extent. The hardness distribution is related to the microstructure of different regions.

2.4 Tensile strength and fracture analysis

Results of tensile tests for BM and welded joints are shown in Table 3, and the data in Table 3 are the average of three measurements. The corresponding stress-strain curves are shown in Fig.9. The incomplete penetration is generated to joint 4#, as shown in Fig.2(h). Consequently, the mechanical property of joint 4# decreases greatly, and it has the lowest tensile strength of 262.1 MPa. Un-

Table 3 Results of tensile tests for BM and welded joints

Sample No.	BM	1#	2#	3#	4#	5#
Tensile strength /MPa	545.0	352.1	369.4	345.6	262.1	340.2
Elongation /%	6.5	1.5	1.6	1.5	1.2	1.4

der the appropriate welding parameters, the tensile strength of joint 2# is the maximum. It reaches 369.4 MPa, which is 67.8% of that of BM. In present work, the appropriate welding parameters are as follows: 4.5 kW of laser power, 3.5 m/min of welding speed, and 5 m/min of wire feeding speed.

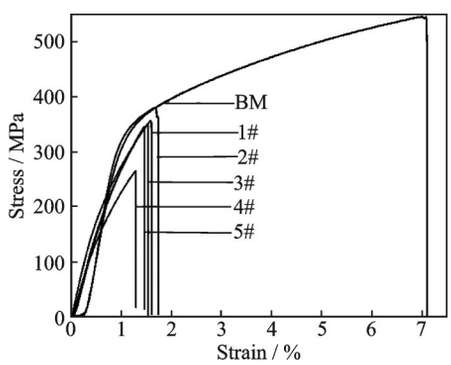

Fig.9 Stress-strain curves of BM and welded joints

Compared with that of BM, the tensile strength of the welded joint decreases to a certain extent. In AW condition, the weld metal is under-aging, and the quantity of strengthening phases precipitated in FZ is insufficient, while HAZ is over-aged. The joint fails in weldment during stretching, and FZ is the weak area of the joint. It is consistent with the microhardness distribution in weld zone.

From Table 3, the elongation of the welded joint is relatively low. The similar results were also obtained in some Refs.[18-19]. It is probably that the heat treatment condition of BM is T8 and the welded joint is in the AW condition. The ductility of joints mainly depends on their chemical composition and heat treatment condition. After appropriate post-weld heat treatment (PWHT), the ductility of the welded joint can be improved to a certain extent.

The tensile fracture morphology of joint 2# is shown in Fig.10. Fig.10(a) shows the overall morphology of the fracture surface. There are a large number of equiaxed dimples on the fracture surface, and some secondary phase particles distribute inside the dimples, as shown in Fig.10(g). The tearing edges appear in the local area of fracture, as shown

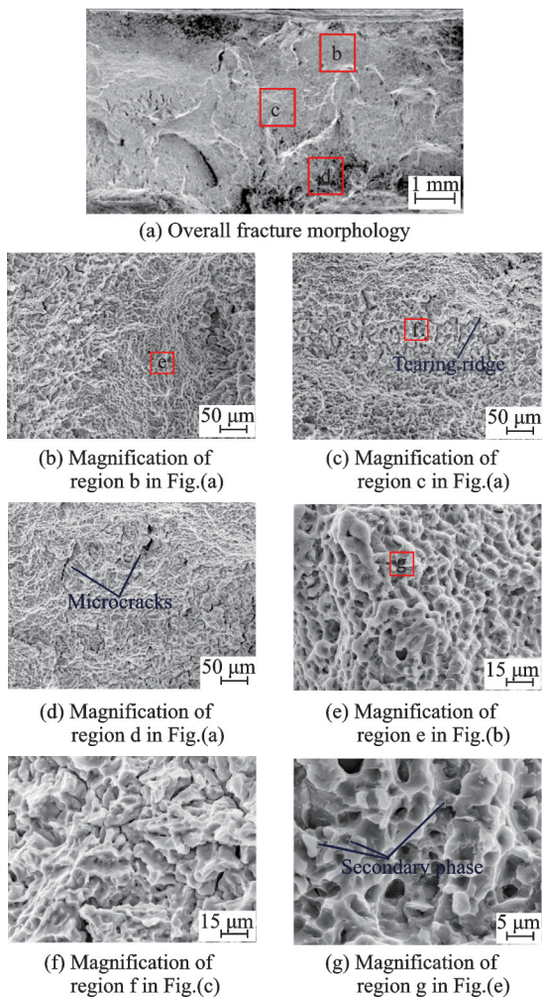

(a) Overall fracture morphology
(b) Magnification of region b in Fig.(a)
(c) Magnification of region c in Fig.(a)
(d) Magnification of region d in Fig.(a)
(e) Magnification of region e in Fig.(b)
(f) Magnification of region f in Fig.(c)
(g) Magnification of region g in Fig.(e)

Fig.10 SEM images of the joint tensile fracture

in Fig.10(c). The tensile fracture of joint is characterized by the intergranular fracture of dimple aggregation. As described above, there are eutectic structures and secondary phase particles at grain boundaries. During the tensile process, dislocations are accumulated around the eutectic structure, which leads to the local stress concentration. When the external stress exceeds the ultimate tensile strength of eutectic structure at grain boundary, micro-pores will be generated. Subsequently, they gradually change into microcracks, as shown in Fig.10(d). With the increase of the tensile stress, microcracks will expand along the eutectic structure at grain boundary, which leads to the joint fracture finally.

3 Conclusions

(1) Under the appropriate welding parameters, by the addition of Al-Si welding wire during the LBW process, the joint with good morphology

is obtained. In present work, the optimized welding parameters are as follows: 4.5 kW of laser power, 3.5 m/min of welding speed, and 5 m/min of wire feeding speed.

(2) During the welding of the Al-Cu-Li alloy, alloying elements Cu and Si are prone to aggregation at grain boundaries. By the addition of Al-Si filler wire, the weld formation and the distribution of precipitated phases improve obviously.

(3) There are mainly α-Al matrix phase and some strengthing phases such as T_1 (Al_2CuLi), T(AlLiSi), δ'(Al_3Li), θ'(Al_2Cu) and β'(Al_3Zr) in weldment. Under the appropriate welding parameters, the tensile strength of the welded joint reaches 369.4 MPa, which is 67.8% of BM. There are many equiaxed dimples on the fracture surface, and the joint mainly presents the fracture characteristic of dimple aggregation.

References

[1] RIOJA R J, LIU J. The evolution of Al-Li base products for aerospace and space applications[J]. Metallurgical and Materials Transactions A, 2012, 43(9): 3325-3337.

[2] MUTHUMANICKAM A, GANDHAM P, DHENUVAKONDA S. Effect of friction stir welding parameters on mechanical properties and microstructure of AA2195 Al-Li alloy welds[J]. Transactions of the Indian Institute of Metals, 2019, 72(6): 1557-1561.

[3] GIALOS A A, ZEIMPEKIS V, ALEXOPOULOS N D, et al. Investigating the impact of sustainability in the production of aeronautical subscale components[J]. Journal of Cleaner Production, 2018, 176: 785-799.

[4] SUN Peng, ZHANG Ting, ZHANG Yanan. Laser welding technology on high-silicon aluminum alloy and its welded joint[J]. Journal of Nanjing University of Aeronautics and Astronautics, 2019, 51(S): 44-49. (in Chinese)

[5] HAO X Q, LI L, SONG X L, et al. Mechanical properties of laser welded joints of high volume fraction SiCp/Al aluminum matrix composite[J]. Transactions of Nanjing University of Aeronautics and Astronautics, 2018, 35(3): 522-528.

[6] OLIVEIRA J P, SCHELL N, ZHOU N, et al. Laser welding of precipitation strengthened Ni-rich NiTi-Hf high temperature shape memory alloys: Microstructure and mechanical properties[J]. Materials and Design, 2019, 162: 229-234.

[7] OLIVEIRA J P, SHEN J J, ESCOBAR J D, et al. Laser welding of H-phase strengthened Ni-rich NiTi-20Zr high temperature shape memory alloy[J]. Materials and Design, 2021, 202: 109533.

[8] OLIVEIRA J P, SHEN J J, ZENG Z, et al. Dissimilar laser welding of a CoCrFeMnNi high entropy alloy to 316 stainless steel[J]. Scripta Materialia, 2022, 206: 114219.

[9] EXAMILIOTI T N, KASHAEV N, ENZ J, et al. On the influence of laser beam welding parameters for autogenous AA2198 welded joints[J]. The International Journal of Advanced Manufacturing Technology, 2020, 110: 2079-2092.

[10] GU C, WEI Y H, ZHAN X H, et al. Investigation of welding parameters on microstructure and mechanical properties of laser beam-welded joint of 2060 Al-Cu-Li alloy[J]. The International Journal of Advanced Manufacturing Technology, 2017, 91: 771-780.

[11] CUI L, LI X Y, HE D Y, et al. Effect of Nd:YAG laser welding on microstructure and hardness of an Al-Li based alloy[J]. Materials Characterization, 2012, 71: 95-102.

[12] LIU T, ZHANG Y Q, KANG Y, et al. Effect of micro morphology in different zones on mechanical properties of 2060 Al-Li alloy laser welded joints[J]. Journal of Manufacturing Processes, 2020, 50: 336-344.

[13] XIAO R S, ZHANG X Y. Problems and issues in laser beam welding of aluminum-lithium alloys[J]. Journal of Manufacturing Processes, 2014, 16: 166-175.

[14] ENZ J, CARRARIN C, RIEKEHR S, et al. Hot cracking behaviour of an autogenously laser welded Al-Cu-Li alloy[J]. The International Journal of Advanced Manufacturing Technology, 2018, 95: 229-310.

[15] JAN R, HOWELL P R, MARTUKANITZ R P. Optimizing the parameters for laser beam welding of aluminum-lithium alloy 2195[C]//Proceedings of the 4th International Conference on Trends in Welding Research. Ohio: ASM, 1996: 329-334.

[16] LUKIN V I, SKUPOV A A, IODA E N. Investigation of the weldability of an aluminium-lithium alloy[J]. Welding International, 2018, 32(3): 214-218.

[17] ZHANG X Y, HUANG T, YANG W X, et al. Microstructure and mechanical properties of laser beam-welded AA2060 Al-Li alloy[J]. Journal of Materials Processing Technology, 2016, 237: 301-308.

[18] HAN B, TAO W, CHEN Y B, et al. Double-sided laser beam welded T-joints for aluminum-lithium alloy aircraft fuselage panels: Effects of filler elements on microstructure and mechanical properties[J]. Optics

and Laser Technology, 2017, 93: 99-108.
[19] ZHANG X Y, YANG W X, XIAO R S. Microstructure and mechanical properties of laser beam welded Al-Li alloy 2060 with Al-Mg filler wire[J]. Materials and Design, 2015, 88: 446-450.
[20] REDDY G M, GOKHALE A A, PRASAD K S, et al. Chill zone formation in Al-Li alloy welds[J]. Science and Technology of Welding and Joining, 1998, 3(4): 208-212.
[21] GUTIERREZ A, LIPPOLD J C. A proposed mechanism for equiaxed grain formation along the fusion boundary in aluminum-copper-lithium alloys[J]. Welding Journal, 1998, 77(3): 123-132.
[22] FU B L, QIN G L, MENG X M, et al. Microstructure and mechanical properties of newly developed aluminum-lithium alloy 2A97 welded by fiber laser[J]. Materials Science and Engineering A, 2014, 617: 1-11.
[23] ZHOU Baosheng, LIU Fencheng, HUANG Chunping, et al. Microstructure and properties of laser beam welded 2060 Al-Li alloys filled with ER4047 wire[J]. Rare Metal Materials and Engineering, 2018, 47(7): 2216-2224. (in Chinese)
[24] CHEN G Q, YIN Q X, ZHANG G, et al. Fusion-diffusion electron beam welding of aluminum-lithium alloy with Cu nano-coating[J]. Materials and Design, 2020, 188: 108439.
[25] CHEN G Q, YIN Q X, ZHANG G, et al. Underlying causes of poor mechanical properties of aluminum-lithium alloy electron beam welded joints[J]. Journal of Manufacturing Processes, 2020, 50: 216-223.

Acknowledgement This work was supported by the Key Research and Development Program of Zhenjiang City (No. GY2019004).

Authors Mr. **LI Kang** received the B.S. degree from Nanjing Tech University in 2019. He joined in Nanjing University of Aeronautics and Astronautics in September 2019. His research is focused on the laser welding technology of Al-Li alloy.

Dr. **WANG Shaogang** received the B.S. degree from Nanchang Institute of Aeronautical Technology in 1990 and Ph.D. degree from Nanjing University of Aeronautics and Astronautics in 2006, respectively. Now he is an associate professor in College of Materials Science and Technology, Nanjing University of Aeronautics and Astronautics. His research is focused on the welding technology of advanced materials.

Author contributions Mr. **LI Kang** conducted the experiment and microstructure analysis, interpreted the results and wrote the original manuscript. Dr. **WANG Shaogang** designed the study, revised and polished the manuscript. Mr. **HU Bingzhou** contributed to the property measurement and experimental preparation. All authors commented on the manuscript draft and approved the submission.

Competing interests The authors declare no competing interests.

(Production Editor: XU Chengting)

Al-Cu-Li合金激光填丝焊接头的组织与性能

李 康，王少刚，胡冰周

(南京航空航天大学材料科学与技术学院，南京 211106，中国)

摘要：采用ER4043焊丝作为填充材料对Al-Cu-Li合金进行激光填丝焊接。系统研究了焊接接头的显微组织与力学性能。微观分析显示，接头焊缝区主要为α-Al基体相以及一些强化相T、δ′、θ′、β′和T_1等。焊接时通过添加Al-Si焊丝，焊缝成形和接头质量明显改善。接头的力学性能测试表明，与母材(Base metal, BM)相比，焊接区的显微硬度有所降低。在合适的焊接参数条件下，获得接头的抗拉强度为369.4 MPa，达母材抗拉强度的67.8%。接头拉伸断口表面分布有许多韧窝，接头整体上呈韧窝聚集型断裂特征。

关键词：Al-Cu-Li合金；激光填丝焊；微观结构；力学性能